

This is an Open Access document downloaded from ORCA, Cardiff University's institutional repository: <https://orca.cardiff.ac.uk/id/eprint/119193/>

This is the author's version of a work that was submitted to / accepted for publication.

Citation for final published version:

Sarma, Plaban Jyoti, Dey Baruah, Satyajit, Logsdail, Andrew and Deka, Ramesh Chandra 2019. Hydride pinning pathway in the hydrogenation of CO<sub>2</sub> into formic acid on dimeric tin dioxide. *ChemPhysChem* 20 (5) , pp. 680-686.  
10.1002/cphc.201801194

Publishers page: <http://dx.doi.org/10.1002/cphc.201801194>

Please note:

Changes made as a result of publishing processes such as copy-editing, formatting and page numbers may not be reflected in this version. For the definitive version of this publication, please refer to the published source. You are advised to consult the publisher's version if you wish to cite this paper.

This version is being made available in accordance with publisher policies. See <http://orca.cf.ac.uk/policies.html> for usage policies. Copyright and moral rights for publications made available in ORCA are retained by the copyright holders.



# Hydride Pinning Pathway in the Hydrogenation of CO<sub>2</sub> into Formic Acid on Small Tin Dioxide Clusters

Plaban Jyoti Sarma,<sup>[a]</sup> Satyajit Dey Baruah,<sup>[a]</sup> Andrew Logsdail<sup>[b]</sup> and Ramesh Chandra Deka<sup>\*[a]</sup>

**Abstract:** Capture of CO<sub>2</sub>, and conversion into organic feedstocks, are of increasing need as society moves to a renewable energy economy. Here, a hydride assisted selective reduction pathway is proposed for the conversion of CO<sub>2</sub> to formic acid (FA) over SnO<sub>2</sub> monomer and dimer. Our density functional theory (DFT) calculations infer the strong chemisorption of CO<sub>2</sub> on SnO<sub>2</sub> clusters by forming a carbonate structure, whereas heterolytic cleavage of H<sub>2</sub> provides a new pathway for the selective reduction of CO<sub>2</sub> to formic acid at low overpotential. Among two investigated pathways for reduction of CO<sub>2</sub> to HCOOH, the hydride pinning pathway is found promising with a unique selectivity for HCOOH. The negatively-charged hydride forms on the cluster during the dissociation of H<sub>2</sub> and facilitates the formation of formate intermediate, which determines the selectivity for FA over alternative CO and H<sub>2</sub> evolution reaction. It is confirmed that SnO<sub>2</sub> clusters exhibit different catalytic behaviour than surface equivalents, thus offering promise for future work investigating the reduction of CO<sub>2</sub> to FA via a hydride pinning pathway at low overpotential and CO<sub>2</sub> capturing.

## Introduction

CO<sub>2</sub> is a color- and odor-less gas that contributes significantly to the phenomenon of global warming. Consumption of fossil fuels and various anthropogenic sources has led to the ceaseless emission of CO<sub>2</sub> pertaining to both short and long-term threat to the mankind and all alike.<sup>[1,2]</sup> Therefore, there has been sustained academic and commercial attempts to improve current methods of conversion or trapping of this potent greenhouse gas. Conversion of CO<sub>2</sub> into valuable chemicals such as HCOOH, CH<sub>3</sub>OH, CO etc. is desirable due to their individual applications.<sup>[3-6]</sup> Among them, reduction of CO<sub>2</sub> into formic acid and methanol opens the route for the storage and transportation of H<sub>2</sub>, which itself is considered a fuel of the future. Hence, both HCOOH and MeOH can serve as potential liquid chemical hydrogen storage (CHS) materials.<sup>[7]</sup> Additionally, HCOOH exists as a liquid at room temperature and can be used in a direct formic acid fuel cell.<sup>[8]</sup> Apart from that, HCOOH would prove to be more beneficial compared to other organic feedstocks due to nontoxic nature as well as ease in transportability. However, the conversion process which is critical because of its thermodynamic stability (C=O bond

about the activation of CO<sub>2</sub>.<sup>[9]</sup> There are several possible methods by which CO<sub>2</sub> reduction can be performed, such as catalytic hydrogenation; complex metal hydrides, electrochemical reduction, photocatalysis and biological reduction. Among these methods, electro- and photo-chemical reduction of CO<sub>2</sub> to HCOOH are promising because of their high efficiency, product selectivity and lower production cost.<sup>[10-12]</sup>

Recently, Sn-based electrodes have gained popularity as a suitable catalyst because of their low toxicity and price for large-scale application.<sup>[13,14]</sup> Tin electrodes show relatively high overpotential resulting from the higher Tafel slope value (254 mV dec<sup>-1</sup>) for the H<sub>2</sub> evolution reaction, a major competing reaction with the HCOOH formation, making the catalyst more selective towards the reduction of CO<sub>2</sub> to FA.<sup>[15]</sup> Like other non-noble metal electrodes, Sn electrodes also undergo corrosion and degradation, which leads to the deactivation of the catalyst,<sup>[16]</sup> but the effect tends to be good for Sn because the oxide layer is also catalytically active for the CO<sub>2</sub> reduction. Chen and Kanan have studied the importance of the oxide layer in the mechanism and reported that catalytic activity in presence of the oxide layer is proportional to the reduction efficiency.<sup>[17]</sup>

Numerous experimental studies have focused on the selective CO<sub>2</sub> electroreduction to formic acid using tin dioxide nanoparticles.<sup>[18-20]</sup> Meyer and co-workers investigated that by controlling nanoparticle size, a high current density of >10 mA/cm<sup>2</sup>, corresponding to formate production, can be achieved at a lower overpotential of ~340 meV.<sup>[21]</sup> In another study, Kumar et al. discussed the activity of reduced SnO<sub>2</sub> nanowires towards the selectivity for HCOOH.<sup>[22]</sup> They revealed that the nanoporous nature and high numbers of grain boundaries of the particles are major factors in the enhancement of the rate and selectivity of HCOOH production. In comparison with the experimental studies theoretical investigations on the proper mechanism of CO<sub>2</sub> reduction to formic acid over SnO<sub>2</sub> catalyst are few. In the reported literature, the mechanism is initiated by the activation of CO<sub>2</sub>, where the chemisorption of CO<sub>2</sub> results in a change of structure from linear to bent. After that, successive addition of 'H' to the CO<sub>2</sub> leads to the formation of formic acid. Moreover, the transfer of 'H' to the 'C' or 'O' of the CO<sub>2</sub> will determine the selectivity for the HCOOH or CO respectively.<sup>[23]</sup> Cui et al. explained the effect of surface hydroxyls on the reduction mechanism, where they promote the formation of HCOOH as a major product.<sup>[24]</sup> All these studies are relevant to the SnO<sub>2</sub> surface, but the mechanism on small sized tin dioxide, where quantum confinement and morphology are influential, remains unknown. The controlled synthesis of ~0.5-2.5 nm SnO<sub>2</sub> quantum dots is reported by Xu et al. and studied their catalytic behaviour towards ethanol sensing. They observed that the SnO<sub>2</sub> QDs shows higher sensitivity than relatively higher sized SnO<sub>2</sub> nanowires.<sup>[25]</sup> In addition, SnO<sub>2</sub> particles are also synthesized in gas phase via detonation process where Yan and coworkers reported the lowest diameters of the particle is 1 nm.<sup>[26]</sup> Therefore, in our current study, we aim to predict the global minimum structure of SnO<sub>2</sub> and Sn<sub>2</sub>O<sub>4</sub> clusters and investigate their catalytic behaviour towards hydrogenation of CO<sub>2</sub>. We identified that the growth of the nanocluster is different from the bulk and

[a] Mr. Plaban Jyoti Sarma, Mr. Satyajit Dey Baruah, Prof. Ramesh Chanda Deka  
Department of Chemical Sciences  
Tezpur Univeresity  
Napaam, Sonitpur, Assam, India-784018  
E-mail: ramesh@tezu.ernet.in

[b] Dr. Andrew Logsdail  
School of Chemistry  
Cardiff Catalysis Institute, Cardiff University, Cardiff CF10 3AT, UK

Supporting information for this article is given via a link at the end of the document.

energy ~533 kJ/mol), requires a suitable catalyst that can bring

hence the catalytic properties are also different from bulk and the surface.

Selective CO<sub>2</sub> reduction to formic acid has also been studied on other metal clusters,<sup>[27,28]</sup> metal complexes,<sup>[29]</sup> ionic liquids,<sup>[30]</sup> transition metal surfaces,<sup>[31,32]</sup> metal-hydride<sup>[33,34]</sup> and surfaces of In<sub>2</sub>O<sub>3</sub>, CeO<sub>2</sub>, ZnO etc.<sup>[12,35-37]</sup> On the Cu-hydride nanocluster, CO<sub>2</sub> reduction follows a different mechanism where CO<sub>2</sub> get activated in the influence of lattice hydride and forms formate intermediate at an overpotential of 0.32 eV.<sup>[38]</sup> This investigation paves a new way of thinking about the hydride assisted pathway for the selective reduction CO<sub>2</sub> to FA over metal oxide nanoparticles; we have built our understanding around the interaction of CO<sub>2</sub> and dissociation of H<sub>2</sub> on small SnO<sub>2</sub> monomer and dimer, and subsequently investigated a new and selective path for the conversion of CO<sub>2</sub> into formic acid.

## Results and Discussion

### Global minimum structures of SnO<sub>2</sub> and Sn<sub>2</sub>O<sub>4</sub> cluster.

Structures of both SnO<sub>2</sub> and Sn<sub>2</sub>O<sub>4</sub> clusters are optimized at MN12-SX/def2TZVPP level of theory (Figure 1). For SnO<sub>2</sub> cluster only a single isomer is found whereas for Sn<sub>2</sub>O<sub>4</sub> we are reporting three low lying configurational isomer and they are presented in Fig. S1. Both GM structures are symmetric and fall in the 'D' group. SnO<sub>2</sub> cluster provides only one binding sites (Sn-O) for the guest molecule whereas the dimeric Sn<sub>2</sub>O<sub>4</sub> structure offers two binding sites, the terminal 'Sn-O' and the bridging 'Sn-O' site. On the basis of the information as discussed, in the next sections we describe the adsorption of CO<sub>2</sub> and dissociation of H<sub>2</sub> on both of these clusters, followed by the reduction mechanism of CO<sub>2</sub>.

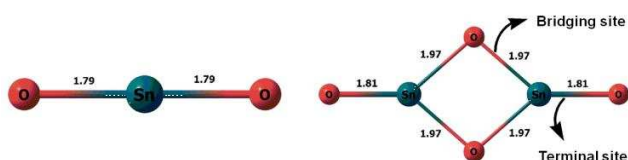


**Figure 1.** DFT optimized structure of SnO<sub>2</sub> and Sn<sub>2</sub>O<sub>4</sub> cluster along with their symmetry point group and structural parameters.

### Adsorption of CO<sub>2</sub> on SnO<sub>2</sub> and Sn<sub>2</sub>O<sub>4</sub> clusters.

Optimized geometries illustrating the chemisorption behaviour of CO<sub>2</sub>, on all the possible sites of both clusters, are given in Figure 2. For SnO<sub>2</sub>, the CO<sub>2</sub> takes the form of carbonate structure after chemisorption, where 'O' of the CO<sub>2</sub> binds with the Sn-center and 'C' makes bond to 'O' of the cluster. The chemisorption on metal oxides of CO<sub>2</sub> has been observed to result in carbonate formation in the previous studies by Cui et al.<sup>[24]</sup> The differences in C=O bond length and CO<sub>2</sub> bond angle for the transition state and chemisorbed structures also demonstrates the activation of CO<sub>2</sub> on the SnO<sub>2</sub> cluster. The characteristic Sn-O bond length changes from 1.84 Å in transition state to 1.97 Å in the chemisorbed SnO<sub>2</sub>CO<sub>2</sub>-C and Sn<sub>2</sub>O<sub>4</sub>CO<sub>2</sub>-C<sub>T</sub>, while in the Sn<sub>2</sub>O<sub>4</sub>CO<sub>2</sub>-C<sub>B</sub>, the parent 'Sn-O' bond dissociates and forming a new 'Sn-O' bond with the 'O' of CO<sub>2</sub> maintaining a bond distance of 1.96 Å. (vdWc= van der Waals complex, C=Chemisorption, T=Terminal position, B=Bridging position). At the same time, the C-O bond elongates from 1.21 Å to 1.34-1.36 Å once CO<sub>2</sub> is bonded to the cluster. In addition, the ∠O-C-O bond angle changes from 148°-157° in TS to the range of 121°-126° in chemisorbed clusters, which is also

satisfying the chemisorbed range for CO<sub>2</sub> and correlating with reported activation range of CO<sub>2</sub>.<sup>[24,37]</sup> From this scenario, we can clearly see that the process of CO<sub>2</sub> activation occurs when the dimensionality of the molecule changes from linear to a planer carbonate structure.

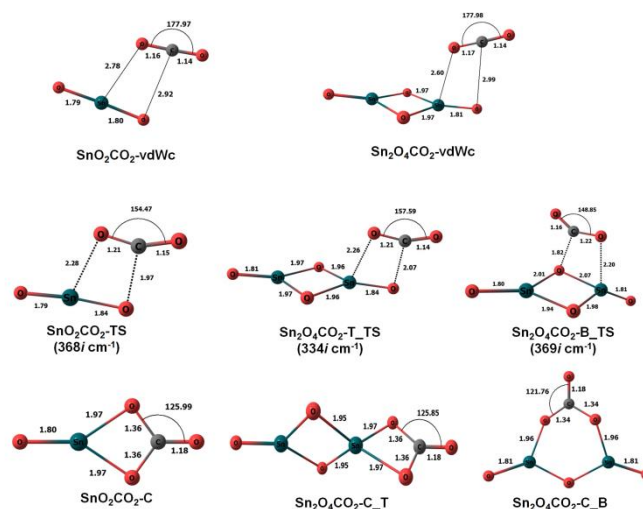


**Figure 2.** MN12-SX optimized structures of van der Waals complexes of CO<sub>2</sub> interaction as SnO<sub>2</sub>CO<sub>2</sub>-vdWc and Sn<sub>2</sub>O<sub>4</sub>CO<sub>2</sub>-vdWc, chemisorbed CO<sub>2</sub> structures as SnO<sub>2</sub>CO<sub>2</sub>-C, Sn<sub>2</sub>O<sub>4</sub>CO<sub>2</sub>-C<sub>T</sub> and Sn<sub>2</sub>O<sub>4</sub>CO<sub>2</sub>-C<sub>B</sub> and the transition state for the interaction of CO<sub>2</sub> along with the bond length and bond angle. vdWc=van der Waals complex, C=Chemisorption, T=Terminal position, B=Bridging position, TS=Transition state.

Free energies of adsorption and activation energy for the adsorption of CO<sub>2</sub> are calculated to understand the thermodynamic feasibility of the adsorption. The adsorption energy of SnO<sub>2</sub>CO<sub>2</sub>-C is -0.26 eV (-5.98 kcal/mol) with an activation energy of 0.51 eV (11.84 kcal/mol), whereas, for Sn<sub>2</sub>O<sub>4</sub>CO<sub>2</sub>-C<sub>T</sub> and Sn<sub>2</sub>O<sub>4</sub>CO<sub>2</sub>-C<sub>B</sub> are -0.60 eV (-13.78 kcal/mol) and 0.64 eV (14.76 kcal/mol) respectively. The calculated barrier height values for Sn<sub>2</sub>O<sub>4</sub>CO<sub>2</sub>-C<sub>T</sub> and Sn<sub>2</sub>O<sub>4</sub>CO<sub>2</sub>-C<sub>B</sub> are found 0.39 eV (8.91 kcal/mol) and 0.90 eV (20.77 kcal/mol). These analyses reveal that in both clusters, the terminal position is the suitable site for the adsorption of CO<sub>2</sub> whereas the bridging site is not preferable in Sn<sub>2</sub>O<sub>4</sub>, as a substantial energy of 0.64 eV is required.

### Dissociation of H<sub>2</sub> on SnO<sub>2</sub> and Sn<sub>2</sub>O<sub>4</sub> clusters.

Like CO<sub>2</sub> adsorption, H<sub>2</sub> finds one active site on SnO<sub>2</sub> cluster and two (terminal 'Sn-O' and bridging 'Sn-O') sites for Sn<sub>2</sub>O<sub>4</sub> cluster for dissociation. The clusters with dissociated H<sub>2</sub> are shown in Figure 3.

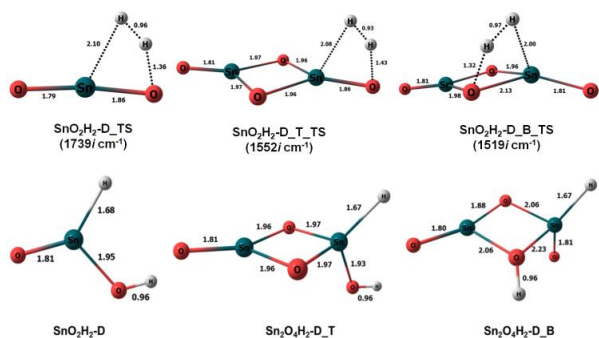


**Figure 3.** Optimized figures of H<sub>2</sub> dissociated clusters along with transition state structures at MN12-SX/def2TZVPP level of theory. (D=Dissociation, T=Terminal and B=bridging).

H<sub>2</sub> dissociation is thermodynamically favourable on both clusters, which is assessed from free energy of dissociation given in Table 1. Along with the dissociated cluster, we are presenting the transition state for the H<sub>2</sub> dissociation on both the clusters. In the monomer the barrier height is calculated 1.48 eV (34.158 kcal/mol) whereas, in dimeric cluster, two transition states are simulated to understand the dissociation nature in the terminal and bridging ‘Sn-O’ site. It is noteworthy to mention that although the barrier height corresponding to the H<sub>2</sub> dissociation in bridging ‘Sn-O’ site is more than in the terminal Sn-O site (table 1) but the elongation of ‘H-H’ bond length is more (0.97 Å) in Sn<sub>2</sub>O<sub>4</sub>-D\_B\_TS than the other two transition states. Therefore, it can be understood that even though the kinetic barrier is little more in Sn<sub>2</sub>O<sub>4</sub>-D\_B\_TS than Sn<sub>2</sub>O<sub>4</sub>-D\_T\_TS but the dissociation is predominant in the bridged position. Besides, in the TS (Sn<sub>2</sub>O<sub>4</sub>-D\_B\_TS), along with the elongation of H-H bond, the bridging ‘Sn-O’ bond also get elongated to 2.13 Å from 1.97 Å in the free Sn<sub>2</sub>O<sub>4</sub> which is a consequence of the substantial activation energy found in Sn<sub>2</sub>O<sub>4</sub>-D\_B\_TS. In the dissociated clusters the formed ‘Sn-H’ bond lengths are 1.68 Å and 1.67 Å in the SnO<sub>2</sub> and Sn<sub>2</sub>O<sub>4</sub> cluster respectively, while, the newly formed O-H bonds are found equal in length in all dissociated sites and that is 0.96 Å. To verify the formation of hydride in each cluster, we have calculated Bader charge of each atom in the chemisorbed structure (Table 1). Bader charges of ‘H’ in SnO<sub>2</sub>H<sub>2</sub>-D, Sn<sub>2</sub>O<sub>4</sub>H<sub>2</sub>-D\_T and Sn<sub>2</sub>O<sub>4</sub>H<sub>2</sub>-D\_B are -0.280, -0.276 and -0.270 e respectively, indicating a gain in electron density. At this point, it is important to describe the structures of the dissociated clusters, since; the reaction mechanism of CO<sub>2</sub> reduction is dependent on the position of the ‘H’ atoms. SnO<sub>2</sub>H<sub>2</sub>-D is planar with the O-H hydrogen pointing out of the plane. In both Sn<sub>2</sub>O<sub>4</sub>H<sub>2</sub>-D\_T and Sn<sub>2</sub>O<sub>4</sub>H<sub>2</sub>-D\_B, the Sn-center takes a distorted tetrahedral arrangement. The analysis of ∠O-Sn-H bond angles is calculated: for Sn<sub>2</sub>O<sub>4</sub>H<sub>2</sub>-D\_T, the ∠O-Sn-H angle, with respect to the bridging O atoms, is ~120°, whereas in Sn<sub>2</sub>O<sub>4</sub>H<sub>2</sub>-D\_B the angles are nearer to ~100° (Figure S2). This indicates the axial orientation of the hydride in Sn<sub>2</sub>O<sub>4</sub>H<sub>2</sub>-D\_B. Another effect associated with the structure of Sn<sub>2</sub>O<sub>4</sub>H<sub>2</sub>-D\_B, that after dissociation the Sn-O(-H) bond length increases to 2.23 Å, as a result of which the hydride tends to orient to axial position with respect to ‘Sn’. To confirm our understanding of the bonding of Sn with hydride, we have also plotted a projected density of states (PDOS) for the atoms involved in ‘Sn-H’ bond (Supporting Information, Figure S2). The PDOS shows stronger interaction of ‘5s’ and ‘5p’ orbitals of Sn with the H ‘1s’ in Sn<sub>2</sub>O<sub>4</sub>H<sub>2</sub>-D\_T than in Sn<sub>2</sub>O<sub>4</sub>H<sub>2</sub>-D\_B. This assessment suggests that the Sn 5s orbitals

are involved in the bonding of ‘Sn-H’ in Sn<sub>2</sub>O<sub>4</sub>H<sub>2</sub>-D\_T, as is also reflected by the larger ∠O-Sn-H bond angle (typically 120° for sp<sup>2</sup> hybridized orbital).

**Table 1.** Free energy of dissociation of H<sub>2</sub> on SnO<sub>2</sub> clusters at 298 K. Also given are the Bader charges of reacting atoms on all the sites of the clusters (D=Dissociation, T=Terminal and B=bridging).

Properties	Bond types	Atoms	SnO <sub>2</sub> H <sub>2</sub> -D	Sn <sub>2</sub> O <sub>4</sub> H <sub>2</sub> -D_T	Sn <sub>2</sub> O <sub>4</sub> H <sub>2</sub> -D_B
Free energy of Dissociation in eV (kcal/mol)			-1.26 (-29.15)	-2.04 (-46.98)	-0.64 (-14.85)
Activation energy eV (kcal/mol)			1.48 (34.18)	1.24 (28.79)	1.52 (35.10)
Bader charge of characteristic atoms  e	(Sn-)H	Sn	1.921	2.162	2.010
		H	-0.280	-0.276	-0.270
	(O-)H	O	-1.249	-1.257	-1.340
		H	0.634	0.641	0.672

### Mechanisms for CO<sub>2</sub> reduction

We have investigated two pathways for the reduction of CO<sub>2</sub> on SnO<sub>2</sub> clusters (Table 2):

- Case I: The formation of formic acid (FA) in a concerted process, where H<sub>2</sub> comes from the gas phase and dissociates on the terminal C=O bond to form FA. Both SnO<sub>2</sub>CO<sub>2</sub>-C and Sn<sub>2</sub>O<sub>4</sub>CO<sub>2</sub>-C\_T are eligible for this mechanism, as adsorption of CO<sub>2</sub> on both clusters is thermodynamically favourable.

- Case II (Hydride Pinning pathway): The step-wise formation of FA via a formate intermediate. Due to the presence of extra Sn-center in the Sn<sub>2</sub>O<sub>4</sub> cluster, this mechanism is only considered for the Sn<sub>2</sub>O<sub>4</sub> cluster: In the first step, the ‘O’ of CO<sub>2</sub> binds to a suitable Sn binding-site and simultaneously the ‘C’ is taking the hydride from the cluster. Then, in the second step, the remaining H is transferred to the unbound O of the adsorbed HCOO\* intermediate.

**Table 2.** Two different Cases that are considered for the formation of HCOOH from reduction of CO<sub>2</sub>

Pathway	Reaction
HCOOH formation case I	CO <sub>2</sub> * + H <sub>2</sub> → HCOOH*
HCOOH formation case II	CO <sub>2</sub> +H* → HCOO* HCOO*+H* → HCOOH

### CO<sub>2</sub> reduction to HCOOH on both SnO<sub>2</sub> and Sn<sub>2</sub>O<sub>4</sub> cluster via Case I.

This mechanism is effectively the direct hydrogenation of CO<sub>2</sub> to Formic acid, with H<sub>2</sub> dissociation taking place on the unbound C=O bond of SnO<sub>2</sub>CO<sub>2</sub>-C and Sn<sub>2</sub>O<sub>4</sub>CO<sub>2</sub>-C\_T. Since the formation of HCOOH does not involve any intermediate, the whole reaction has only one transition state, represented as TS1 and TS2 in Figure 4. These TSs correspond to the formation of HCOOH on SnO<sub>2</sub> and Sn<sub>2</sub>O<sub>4</sub> clusters and are characterized by

the presence of one imaginary frequency of  $2246i\text{ cm}^{-1}$  and  $2249i\text{ cm}^{-1}$ .

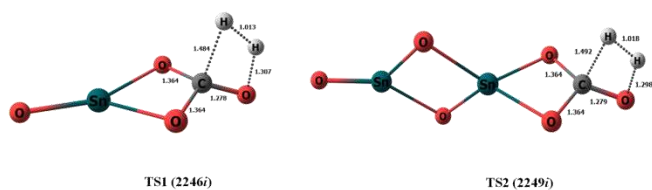


**Figure 4.** Transition states TS1 and TS2 for the formation of HCOOH via case I.

In the transition state, the H••H bond is elongated from  $0.74\text{ \AA}$  to  $1.01\text{ \AA}$  when adsorbed on the cluster. The bond distance of newly formed C••H bonds are  $1.48\text{ \AA}$  and  $1.49\text{ \AA}$ , whereas the O••H bonds are  $1.30\text{ \AA}$  and  $1.29\text{ \AA}$  in TS1 and TS2 respectively. The free energy profile diagram presented in Figures 5, signify the case I pathway for the  $\text{CO}_2$  reduction on  $\text{SnO}_2$  and  $\text{Sn}_2\text{O}_4$  cluster respectively.

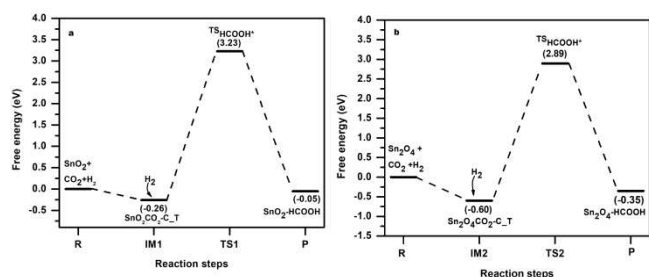


**Figure 5:** Free energy profile for  $\text{CO}_2$  reduction on  $\text{SnO}_2$  (a) and  $\text{Sn}_2\text{O}_4$  (b) clusters via Case I, as calculated at MN12-SX/def2tzvpp level of theory.

From Figure 5, we can see that the free energies of activation for TS1 and TS2 are  $3.492\text{ eV}$  ( $80.54\text{ kcal/mol}$ ) and  $3.490\text{ eV}$  ( $80.50\text{ kcal/mol}$ ), respectively, which is substantial. The difference in energy between the TSs is only  $0.002\text{ eV}$ , so the energetic profiles are very similar for both of the clusters towards catalytic formation of HCOOH via Case I. Clearly, the major drawback of this mechanism is the large energy barrier, which would lead to kinetic infeasibility for the reaction. The high activation energy is attributed to the strong binding of  $\text{CO}_2$  with the clusters; additionally, for the final product, the formed HCOOH binds favourably in a tetrahedral manner with the Sn-center in the cluster, rather than leaving the catalytic site and this could deactivate the catalyst. Thus, we can conclude that  $\text{CO}_2$  reduction is infeasible via this mechanism, though an alternative conclusion is that the strong binding of  $\text{CO}_2$  with the cluster offers promise for application as a carbon dioxide trapping material, which is very important part of  $\text{CO}_2$  mitigation.

#### **$\text{CO}_2$ reduction to HCOOH on $\text{Sn}_2\text{O}_4$ cluster via Case II.**

We have already mentioned while introducing the Case II that the 'Hydride pinning pathway' is only feasible for the  $\text{Sn}_2\text{O}_4$  cluster. Thus, the first question to address is why the monomeric cluster is not a suitable candidate for this mechanism: the lack of a second Sn-center in the cluster limits HCOO formation and hence

formic acid. As a result, rather forming a formate intermediate, carbonate structure is reformed via the chemisorption of  $\text{CO}_2$  (Figure S3). This outcome is due to the unsaturated nature of 'Sn' in  $\text{SnO}_2$  cluster.

In the hydride pinning step over  $\text{Sn}_2\text{O}_4$ , the  $\text{HCOO}^*$  intermediate forms as a result of the transfer of hydride from the  $\text{Sn}_2\text{O}_4$  cluster to the 'C' of  $\text{CO}_2$  and simultaneously the 'O' of  $\text{CO}_2$  binds with another Sn-center in the cluster. Before unraveling the in-depth detailed mechanistic pathway, it is worth mentioning that, even though  $\text{H}_2$  dissociates heterolytically on both terminal and bridging Sn-O sites of the  $\text{Sn}_2\text{O}_4$  cluster, to give  $\text{Sn}_2\text{O}_4\text{H}_2\text{-D}_T$  and  $\text{Sn}_2\text{O}_4\text{H}_2\text{-D}_B$ , the hydride pinning pathway proceeds only via the formation of  $\text{Sn}_2\text{O}_4\text{H}_2\text{-D}_B$ . The reason for this selectivity is attributed to the hydride orientation towards the  $\text{CO}_2$  binding site, whereas the hydride of  $\text{Sn}_2\text{O}_4\text{H}_2\text{-D}_T$  is oriented away from the  $\text{CO}_2$  binding site. These observations strongly suggest that the mechanism proceeds via  $\text{Sn}_2\text{O}_4\text{H}_2\text{-D}_B$ , followed by the hydride pinning step.

A free energy diagram for the overall reaction mechanism is presented in Figure 6. The favorable interaction at the pinning step ( $\text{IM3} \rightarrow \text{IM4}'$ ) is mainly attributed to the attraction of positively charged 'C' of  $\text{CO}_2$  towards the negatively charged hydride. In this step,  $\text{CO}_2$  comes from the gas phase and proceed through a transition state TS3 ( $574i\text{ cm}^{-1}$ ) with an activation energy of  $1.15\text{ eV}$  ( $26.51\text{ kcal/mol}$ ) to take up the hydride from the 'Sn'. In TS3, the C••H and Sn••O distances are  $1.48\text{ \AA}$  and  $2.26\text{ \AA}$ , respectively, whereas the bond length that corresponds to the breaking of Sn••H bond is  $1.81\text{ \AA}$ . The formed  $\text{HCOO}^*$  intermediate ( $\text{IM4}$ ) remains adsorbed on the cluster via one 'O' of  $\text{CO}_2$ , with the unbound 'O' of the  $\text{HCOO}^*$  oriented away from the cluster, however a spontaneous structural transformation occurs with a free energy change ( $\Delta G$ ) of  $-0.52\text{ eV}$  ( $-11.99\text{ kcal/mol}$ ) which gives  $\text{IM4}'$  where, the 'O=C-H' group flips around the Sn-O single bond. Finally,  $\text{IM4}'$  has the (C-)H pointed upward and the unbound 'O' makes a weak stabilizing interaction with the Sn maintaining  $2.38\text{ \AA}$  of bond distance. A major advantage of this structural change is that the weakly bonded 'O' is now nearer to the second hydrogen, which is bonded to one of the bridging 'O' of the cluster. In the last step, the remaining 'H' is transferred to the 'O' and forms HCOOH via a transition state TS4 ( $1003i\text{ cm}^{-1}$ ), with an activation energy of  $0.33\text{ eV}$  ( $7.63\text{ kcal/mol}$ ). In the same step the HCOOH also desorbs from the catalytic site, thus facilitating the regeneration of the catalyst to undergo  $\text{H}_2$  dissociation and repeat the catalytic cycle.

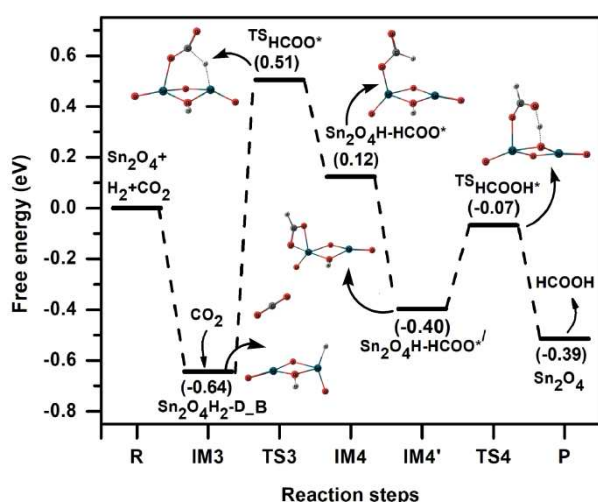


**Figure 6.** Complete potential energy surface diagram for hydride pinning pathway (Case II) for CO<sub>2</sub> reduction calculated at MN12-SX/def2tzvpp level of theory.

After analysis of the free energy diagram, we can clearly state that the pinning step (hydride transfer) is the rate determining step (RDS) of the reaction. Moreover, in this RDS, the  $\Delta G$  difference between the IM3 and IM4' is only 0.24 eV, which is an indicator of the necessary overpotential for HCOOH production vs RHE. Previous experimental studies report the overpotential for HCOOH formation on SnO<sub>2</sub> nanoparticles as 0.34-0.35 eV<sup>[21,22]</sup> and theoretical value reported on copper hydride (Cu<sub>32</sub>H<sub>20</sub>L<sub>12</sub>, L=S<sub>2</sub>PH<sub>2</sub>) nanocluster is 0.32 eV.<sup>[38]</sup> The simulation models and experimental catalysts differ in size but the consistency between results confirms the validity of our approach; furthermore, the subtle differences between experimental and calculated overpotential suggest opportunities to tune the size of the nanoparticle specifically to aid the reduction mechanism of CO<sub>2</sub> to formic acid. The overall reaction cycle for the hydride pinning pathway is shown in Figure 7.

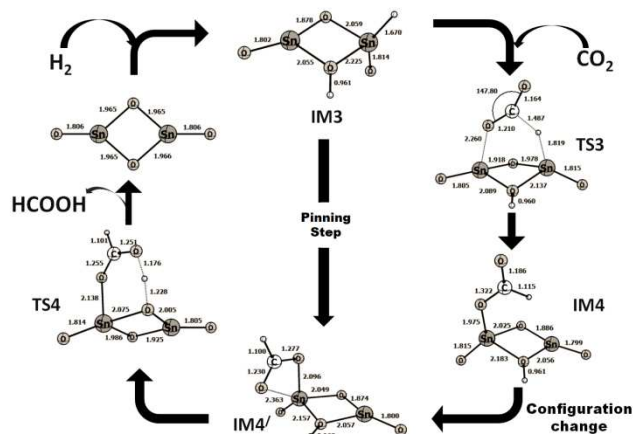


**Figure 7.** Total reaction Cycle of HCOOH formation from CO<sub>2</sub> via hydride pinning pathway.

Thus far, we have discussed the formation of formic acid via the hydride mechanism, but there exist other competing processes such as H<sub>2</sub> evolution reaction and CO formation reactions along with the HCOOH formation. To consider these side reactions, we have studied the H<sub>2</sub> recombination reaction using the Sn<sub>2</sub>O<sub>4</sub>H<sub>2</sub>-D\_B structure as a source for H<sub>2</sub> evolution. The  $\Delta G^\ddagger$  and  $\Delta G$  for the H<sub>2</sub> recombination reaction are found to be 2.17 eV and 0.64 eV, respectively. A free energy diagram, shown in Figure S4 is the comparison between the formate formation and H<sub>2</sub> recombination reactions, alongside the structure of transition state corresponding to the H<sub>2</sub> recombination. Therefore, H<sub>2</sub> recombination will not hinder the HCOOH formation. On the other hand, formation of CO along with H<sub>2</sub>O will be inevitable if the hydride is transferred to the 'O' of CO<sub>2</sub> instead of 'C'. We have substantiated two factors to describe the inhibition of CO formation: 1) the hydride lacks adequate ability to bond with the 'O' of CO<sub>2</sub> as both are negatively charged i.e. coulombic repulsion; 2) there is an absence of a binding site for a COOH intermediate. To confirm this, we have modelled a structure where 'O' of CO<sub>2</sub> takes the 'H' from 'Sn' and forms COOH\* intermediate (SI, Figure S5). We have demonstrated that, after formation of a COOH\* intermediate, reorientation is necessary with adsorption to the cluster via the 'C' atom. This is also observed in previous literature by Tang et al.<sup>[38]</sup> but the bridging oxygens of our cluster are coordinately saturated, so a carbonate structure will be formed if 'C' binds to the terminal 'O' of the cluster, rather picking up the 'H' from the Sn-center to form the COOH intermediate.

## Conclusions

In summary, structures and catalytic activity of SnO<sub>2</sub> atomic clusters are investigated towards the reduction of CO<sub>2</sub> using DFT method. Adsorption of CO<sub>2</sub> on the clusters results in a stable carbonate structure whereas dissociation of H<sub>2</sub> opens a hydride assisted channel for reduction of CO<sub>2</sub> to HCOOH. The stepwise hydride pinning pathway (Case II) is auspicious in determining the selectivity for HCOOH over case I. After the formation of HCOOH, desorption of the product occurs spontaneously and the catalyst active site is regenerated. Using the computational hydrogen

electrode (CHE) model, our results suggest the required overpotential for HCOOH formation is 0.24 eV. The low overpotential is a consequence of having extra Sn-center in the dimer, which plays a crucial role in stabilizing the HCOO\* intermediate. Along with the HCOOH formation, H<sub>2</sub> recombination is also studied and a large activation barrier of 2.12 eV confirms that H<sub>2</sub> evolution is not a major issue in the hydride pinning mechanism. Moreover, the presence of hydride in the cluster inhibits the formation of COOH\* intermediate and therefore, CO formation reaction is not a topic of concern in CO<sub>2</sub> reduction via hydride assisted pathway, as justified via coordination and electrostatic arguments. In the final touch, we put forward two benefits of using SnO<sub>2</sub> nanoclusters: firstly, both clusters are notable at CO<sub>2</sub> trapping material and, secondly, the Sn<sub>2</sub>O<sub>4</sub> cluster serves as a tremendous catalyst with respect to reducing CO<sub>2</sub> to formic acid via the mechanism initiated by H<sub>2</sub> dissociation. These results offer a great platform for further experimental studies to develop our understanding of CO<sub>2</sub> reduction to formic acid via hydride pinning pathway.

## Computational Details

Structures, reaction energies and the detailed mechanism of CO<sub>2</sub> reduction are studied using Kohn-Sham density functional theory (DFT) as available on Gaussian 09 quantum chemistry software package.<sup>[39]</sup> Critical bond dissociation enthalpies of Sn-O, C-O, O-H, C-H, and Sn-H bonds are calculated at 22 tested methods employing density fitting triple- $\xi$  def2TZVPP basis set<sup>[40,41]</sup> as shown in Table S1. The best outcome of the initial analysis is the range-separated hybrid meta-NGA (non-separable gradient approximation) MN12-SX functional<sup>[42]</sup> in describing bond dissociation enthalpies of the bonds close to experimental data. The accuracy of MN12-SX functional agrees with previous studies in predicting both structures and energies.<sup>[43,44]</sup> Along with it, the def2TZVPP basis set proves very good in minimizing the basis set superposition error (BSSE), giving errors of < 0.04 eV, thus providing results close to the DFT basis set limit.<sup>[41]</sup> Therefore, for geometry relaxation and frequency calculation, we have used MN12-SX/def2TZVPP level employing ultrafine integration grid. All reported adsorption and dissociation energies in the manuscript are also corrected appropriately for BSSE. Genetic algorithm is used for global optimization of SnO<sub>2</sub> and Sn<sub>2</sub>O<sub>4</sub> clusters.<sup>[45]</sup> Presence of only one imaginary frequency in the vibrational spectra confirms identified transition states, consistent with the eigenvector along the reaction coordinate, whereas, for the reactant, intermediates, and products, no imaginary frequency is observed, confirming that they are true minima. Gibbs free energy change ( $\Delta G$ ), at 1 atm pressure and 298K temperature are calculated for each step in the reaction mechanisms by referring to the free energy difference between the final and initial states; the calculations for the free energy of adsorption and dissociation at room temperature have been analyzed in a similar manner. The free energy of activation ( $\Delta G^\ddagger$ ) of the transition states are calculated by measuring the free energy change of transition state with respect to the initial state. To gain a more detailed insight into the electronic charge distribution, Bader charge analysis is done using AIMALL software package, verifying the formation of hydride on the H<sub>2</sub> dissociation step.<sup>[46]</sup> As the product (HCOOH) is formed in liquid phase, a correction to the free energy for HCOOH is included in calculating the reaction

energetics, as shown in Supporting Information (Section 1). The computational hydrogen electrode (CHE) model is used to correlate the reaction free energy change with the electrochemical potential, with respect to the transfer of hydrogen from the catalyst to CO<sub>2</sub> while forming the HCOO\* intermediate. At 1 atm, the CHE assumes that the protons and electrons are at equilibrium with the gas phase hydrogen ( $H^+ + e^- \rightarrow 1/2H_2$ ) at potential 0V vs RHE for all pH and all temperature.<sup>[47]</sup>

## Acknowledgements

The authors are thankful to Science & Engineering Research Board (SERB) (EMR/2016/003195), Department of Science and Technology (DST) (No: DST/INSPIRE Fellowship/[IF160658]) New Delhi, India, and Tezpur university for financial support. Authors acknowledge UK-India Education and Research Initiative (UKIERI) for research fund (Grant No. DST/INT/UK/P-35/2012) to carry out collaborative research work. The authors gratefully acknowledge the support of Prof. C. R. A. Catlow, FRS.

**Keywords:** SnO<sub>2</sub> and Sn<sub>2</sub>O<sub>4</sub> cluster, MN12-SX Functional, CO<sub>2</sub> reduction, Formic acid, Hydride Pinning Pathway.

- [1] A. Stips, D. Macias, C. Coughlan, E. Garcia-Goriz, X. S. Liang, *Sci. Rep.* **2016**, *6*, 21691–21699.
- [2] J. Klankermayer, S. Wesselbaum, K. Beydoun, W. Leitner, *Angew. Chemie - Int. Ed.* **2016**, *55*, 7296–7343.
- [3] S. Roy, B. Sharma, J. Pécaut, P. Simon, M. Fontecave, P. D. Tran, E. Derat, V. Artero, *J. Am. Chem. Soc.* **2017**, *139*, 3685–3696.
- [4] A. Álvarez, A. Bansode, A. Urakawa, A. V. Bavykina, T. A. Wezendonk, M. Makkee, J. Gascon, F. Kapteijn, *Chem. Rev.* **2017**, *117*, 9804–9838.
- [5] Q. Li, J. Fu, W. Zhu, Z. Chen, B. Shen, L. Wu, Z. Xi, T. Wang, G. Lu, J. Zhu, S. Sun, *J. Am. Chem. Soc.* **2017**, *139*, 4290–4293.
- [6] D. Ballivet-Tkatchenko, S. Chambrey, R. Keiski, R. Ligabue, L. Plasseraud, P. Richard, H. Turunen, *Catalysis Today*, **2006**, *115*, 80–87.
- [7] K. Sordakis, C. Tang, L. K. Vogt, H. Junge, P. J. Dyson, M. Beller, G. Laurenczy, *Chem. Rev.* **2018**, *118*, 372–433.
- [8] X. Yu, P. G. Pickup, *Journal of Power Sources*. **2008**, *182*, 124–132.
- [9] A. Bhowmik, T. Vegge, H. A. Hansen, *Chem. Sus. Chem.* **2016**, *9*, 3230–3243.
- [10] J. Wu, Y. Huang, W. Ye, Y. Li, *Adv. Sci.* **2017**, *4*, 1–29.
- [11] A. C. Khezri, M. Fisher, J. Pumera, *Mater. Chem. A* **2017**, *5*, 8230–8246.
- [12] Y. Tamaki, K. Koike, O. Ishitani, *Chem. Sci.* **2015**, *6*, 7213–7221.
- [13] J. Wu, F. G. Risalvato, S. Ma, X. D. Zhou, *J. Mater. Chem. A* **2014**, *2*, 1647–1651.
- [14] J. Medina-Ramos, R. C. Pupillo, T. P. Keane, J. L. Dimeglio, J. Rosenthal, *J. Am. Chem. Soc.* **2015**, *137*, 5021–5027.
- [15] E. Irtem, T. Andreu, A. Parra, M. D. Hernández-Alonso, S. García-Rodríguez, J. M. Riesco-García, G. Penelas-Pérez, J. R. Morante, *J. Mater. Chem. A* **2016**, *4*, 13582–13588.
- [16] G. S. Frankel, A. Agarwal, N. Sridhar, *Electrochim. Acta* **2014**, *133*, 188–196.
- [17] Y. Chen, M. W. Kanan, *J. Am. Chem. Soc.* **2012**, *134*, 1986–1989.
- [18] S. Lee, J. D. Ocon, Y. Son, J. Lee, *J. Phys. Chem. C* **2015**, *119*, 4884–4890.
- [19] W. Lee, N. H. Cho, K. D. Yang, K. T. Nam, *Chem. Electro. Chem.* **2017**, *4*, 2130–2136.
- [20] K. R. Rao, S. Pishgar, J. Strain, B. Kumar, V. Atla, S. Kumari, J. M. Spurgeon, *J. Mater. Chem. A* **2018**, *6*, 1736–1742.
- [21] S. Zhang, P. Kang, T. J. Meyer, *J. Am. Chem. Soc.* **2014**, *136*, 1734–1737.

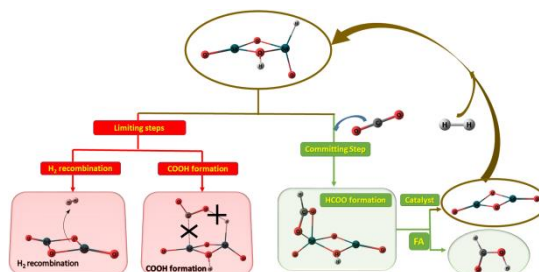
- 
- [22] B. Kumar, V. Atla, J. P. Brian, S. Kumari, T. Q. Nguyen, M. Sunkara, J. M. Spurgeon, *Angew. Chemie - Int. Ed.* **2017**, *56*, 3645–3649.
- [23] K. Saravanan, Y. Basdogan, J. Dean, J. A. Keith, *J. Mater. Chem. A* **2017**, *5*, 11756–11763.
- [24] Cui, J. Han, X. Zhu, X. Liu, H. Wang, D. Mei, Q. Ge, *J. Catal.* **2016**, *343*, 257–265.
- [25] X. Xu, J. Zhuang, X. Wang, *J. Am. Chem. Soc.* **2008**, *130*, 12527–12535.
- [26] Y. Honghao, W. Linsong, L. Xiaojie, W. Xiaohong, *Rare Metal Mat. Eng.* **2013**, *42*, 1325–1327.
- [27] Cai, D. Gao, H. Zhou, G. Wang, T. He, H. Gong, S. Miao, F. Yang, J. Wang and X. Bao, *Chem. Sci.*, **2017**, *8*, 2569–2573.
- [28] C. Liu, H. He, P. Zapol, L. A. Curtiss, *Phys. Chem. Chem. Phys.* **2014**, *16*, 26584–26599.
- [29] T. N. Huan, P. Simon, A. Benayad, L. Guetaz, V. Artero, M. Fontecave, *Chem. Eur. J.* **2016**, *22*, 14029 – 14035.
- [30] T. N. Huan, P. Simon, G. Rousse, I. Genois, V. Artero, M. Fontecave, *Chem. Sci.* **2017**, *8*, 742–747.
- [31] W. Lin, K. M. Stocker, G. C. Schatz, *J. Am. Chem. Soc.* **2017** *139*, 4663–4666.
- [32] C. Liu, T. R. Cundari, A. K. Wilson, *J. Phys. Chem. C* **2012**, *116*, 5681–5688.
- [33] W. Sun, C. Qian, L. He, K. K. Ghuman, A. P. Y. Wong, J. Jia, A. A. Jelle, P. G. O'Brien, L. M. Reyes, T. E. Wood, A. S. Helmy, C. A. Mims, C. V. Singh, G. A. Ozin, *Nat. Commun.* **2016**, *7*, 12553–12561.
- [34] K. M. Waldie, A. L. Ostericher, M. H. Reineke, A. F. Sasayama, C. P. Kubiak, *ACS Catal.* **2018**, *8*, 1313–1324.
- [35] D. Gao, Y. Zhang, Z. Zhou, F. Cai, X. Zhao, W. Huang, Y. Li, J. Zhu, P. Liu, F. Yang, G. Wang, X. Bao *J. Am. Chem. Soc.* **2017**, *139*, 5652–5655.
- [36] X. Zhao, X. Huang, X. Wang, J. Wang, *Mater. Chem. A* **2017**, *5*, 21625–21649.
- [37] X. Lu, W. Wang, S. Wei, C. Guo, Y. Shao, M. Zhang, Z. Deng, H. Zhu, W. Guo, *RSC Adv.* **2015**, *5*, 97528–97535.
- [38] Q. Tang, Y. Lee, D. Y. Li, W. Choi, C. W. Liu, D. Lee, D. E. Jiang, *J. Am. Chem. Soc.* **2017**, *139*, 9728–9736.
- [39] M. J. Frisch, G. W. Trucks, H. B. Schlegel, G. E. Scuseria, M. A. Robb, J. R. Cheeseman, G. Scalmani, V. Barone, B. Mennucci, G. A. Petersson, H. Nakatsuji, M. Caricato, X. Li, H. P. Hratchian, A. F. Izmaylov, J. Bloino, G. Zheng, J. L. Sonnenberg, M. Hada, M. Ehara, K. Toyota, R. Fukuda, J. Hasegawa, M. Ishida, T. Nakajima, Y. Honda, O. Kitao, H. Nakai, T. Vreven, J. A. Montgomery, Jr., J. E. Peralta, F. Ogliaro, M. Bearpark, J. J. Heyd, E. Brothers, K. N. Kudin, V. N. Staroverov, R. Kobayashi, J. Normand, K. Raghavachari, A. Rendell, J. C. Burant, S. S. Iyengar, J. Tomasi, M. Cossi, N. Rega, J. M. Millam, M. Klene, J. E. Knox, J. B. Cross, V. Bakken, C. Adamo, J. Jaramillo, R. Gomperts, R. E. Stratmann, O. Yazyev, A. J. Austin, R. Cammi, C. Pomelli, J. W. Ochterski, R. L. Martin, K. Morokuma, V. G. Zakrzewski, G. A. Voth, P. Salvador, J. J. Dannenberg, S. Dapprich, A. D. Daniels, Ö. Farkas, J. B. Foresman, J. V. Ortiz, J. Cioslowski, and D. J. Fox, Gaussian09 Revision D.01, Gaussian Inc. Wallingford CT. **2010**.
- [40] F. Weigend, *Phys. Chem. Chem. Phys.* **2006**, *8*, 1057–1065.
- [41] F. Weigend, R. Ahlrichs, *Phys. Chem. Chem. Phys.* **2005**, *7*, 3297–3305.
- [42] R. Peverati, D. G. Truhlar, *Phys. Chem. Chem. Phys.* **2012**, *14*, 16187–16191.
- [43] J. Frau, D. Glossman-Mitnik, *Theor. Chem. Acc.* **2018**, *137*, 67–76.
- [44] S. Paranthaman, J. Moon, J. Kim, D. E. Kim, T. K. Kim, *J. Phys. Chem. A* **2016**, *120*, 2128–2134.
- [45] M. R. Farrow, Y. Chow, S. M. Woodley, *Phys. Chem. Chem. Phys.* **2014**, *16*, 21119–21134.
- [46] AIMAll (Version 17.11.14), Todd A. Keith, TK Gristmill Software, Overland Park KS, USA, **2017** (aim.tk.gristmill.com).
- [47] J. K. Nørskov, J. Rossmeisl, A. Logadottir, L. Lindqvist, J. R. Kitchin, T. Bligaard, H. Jónsson, *J. Phys. Chem. B* **2004**, *108*, 17886–17892.



## FULL PAPER

Text for Table of Contents

**Representation of different paths involved in the hydrogenation of CO<sub>2</sub> to formic acid:** The modelled Sn<sub>2</sub>O<sub>4</sub> cluster has shown a unique selectivity towards HCOOH when the mechanism proceeds via hydride assisted pathway (committing step) over CO formation and H<sub>2</sub> recombination reactions (limiting steps).



*Plaban Jyoti Sarma, Satyajit Dey Baruah, Andrew Logsdail, Ramesh Chandra Deka\**

**Page No. – Page No.**

**Hydride Pinning Pathway in the Hydrogenation of CO<sub>2</sub> into Formic Acid on Small Tin Dioxide Clusters**